On the relation between the spatial dose integrity and the temporal instability of polymer gel dosimeters

K Vergote[1]**, Y De Deene**[1]**, E Vanden Bussche and C De Wagter**

Department of Radiotherapy, Ghent University Hospital, De Pintelaan 185, 9000 Gent, Belgium

E-mail: koen.vergote@ugent.be

Abstract

When irradiating a polymer gel dosimeter to relatively high doses, edge enhancing effects (overshoots) may be noticed near dose gradients, resulting in a loss of spatial dose integrity. These overshoots are believed to be a consequence of monomers diffusing into the high-dose region, where they react with long-living macroradicals. Macroradicals may also be responsible for the temporal chemical instability of post-irradiation polymerization that occurs in the polymer gel dosimeter. In this study, a mathematical model is proposed that simulates the edge enhancing effect. The model is based on the hypothesis that the macroradicals are responsible for both the temporal instability and loss of spatial dose integrity. All input parameters for the model are obtained from independent experiments. The edge enhancing effect is studied both experimentally and theoretically for polymer gel dosimeters with various gelatin concentrations. The change in the edge enhancement is also investigated over post-irradiation time. Comparisons between polymer gel measurements and simulations confirm the hypothesis that there is a strong relation between the spatial and temporal instabilities.

1. Introduction

Due to the increasing complexity of radiotherapy treatment planning and delivery, accurate experimental radiation dosimetry plays an important role in the implementation and quality assurance of new treatment techniques. In 1993, Maryanski *et al* introduced polymer gel dosimetry as a new dosimetric tool that enables dose measurements in three dimensions with high spatial accuracy (Maryanski *et al* 1993). The gel dosimeter is composed of an

---

[1] Both authors contributed equally to this paper.

oxygen-free hydrogel in which monomers—originally acrylamide (AA) and N,N′-methylene-bisacrylamide (Bis)—are dissolved. When irradiated, radiolysis of water molecules produces radicals that initiate a free-radical co-polymerization reaction. The amount of polymer formed at a specific location in the gel is a function of the locally absorbed dose. The polymer aggregates affect the local spin–spin relaxation rate (R2) of the gel. Therefore, magnetic resonance imaging (MRI) can be used to visualize the absorbed dose distribution in the gel dosimeter.

Shortly after the introduction of polymer gel dosimeters, edge enhancing effects (overshoots) were noticed in the gel near high-dose gradient regions, at relatively high-dose levels (Maryanski *et al* 1994). A high-dose region in the gel results in a local depletion of monomers. Monomers from the low dose region that diffuse into the high-dose region react with long-living polymer macroradicals that are created in the high-dose region. As a result, an overshoot in the measured dose distribution can occur near the edge of the high-dose region. Our research group has also reported these spatial instabilities in several other studies (De Deene *et al* 1998a, 2001, Vergote *et al* 2004). De Deene *et al* (2002) also noticed that the overshoot amplitude is dependent on the post-irradiation time. Although the diffusion hypothesis as described above is generally accepted, it has never been substantiated.

When evaluating the dose response of the polymer gel after irradiation, two types of temporal instabilities are observed (De Deene *et al* 2000). In the first few hours after irradiation, the polymerization reaction continues, resulting in an increase in the slope of the dose–R2 response. This prolonged reaction is ascribed to the presence of the long-living macroradicals (Audet 1995, Baldock *et al* 1999) and typically continues up to 12 h after irradiation (De Deene *et al* 2000, Lepage *et al* 2001a) for a polyacrylamide gel (PAG). The second instability is a result of the ongoing gelation of the gelatin, which may continue up to a month after irradiation, and alters the intercept of the dose–response curve (De Deene *et al* 2000, Lepage *et al* 2001b).

In this study, a mathematical model is proposed that is based on the hypothesis that the temporal and spatial instabilities in PAG are both caused by the presence of long-living macroradicals. Experimentally determined parameters are used in the model. Measured R2 distributions of irradiated PAG dosimeters are compared with simulated R2 distributions derived from the model.

2. Materials and methods

2.1. Stability study

A stability study was performed on PAG polymer gels containing different concentrations of gelatin. The dose sensitivity and measured dose profiles were analysed as a function of time.

2.1.1. Gel fabrication. Four batches of PAG gel (3 (w/w)% AA, 3 (w/w)% Bis) were produced with various gelatin concentrations: 0, 3, 6 and 12 (w/w)%. The polymer gels were fabricated according to a procedure described elsewhere (De Deene *et al* 2000). Each batch of polymer gel was divided over a set of 15 test tubes. Each test tube (inner diameter 15 mm, length 100 mm) was filled completely with $\pm$15 ml of polymer gel. In the text, PAG$_x$ refers to a PAG with a gelatin concentration of x (w/w)%.

2.1.2. Irradiation. For each batch of gel, the gel-filled test tubes were irradiated to different known doses (0, 0.25, 0.5, 1, 2, 3, 4, 6, 8, 10, 12.5, 15, 20, 30 and 50 Gy) on a SLiPlus linear accelerator (Elekta, Crawley, UK). Each individual test tube was placed perpendicular to the

beam axis in a dedicated cubic water phantom at a depth of 5 cm at isocentre. For the applied 10×10 cm^2 6 MV photon beam, one monitor unit (MU) then corresponds to an absorbed dose of 1 cGy. Each test tube was placed so that only the bottom half was irradiated. The PAG$_0$ test tubes were placed entirely in the radiation field, because the absence of a gelatin matrix does not allow preservation of spatial variations in the absorbed dose distribution. The applied output rate was always 400 MU min^{-1}. The irradiation took place about 24 h after the polymer gel fabrication.

2.1.3. Scanning. Immediately after irradiation, all test tubes were transferred to the MRI scanner room. A styrofoam framework was produced to position all 60 test tubes in five equidistant planes. Longitudinal cross-sections of the test tubes were scanned at regular time intervals for four weeks on a 1.5 T MRI scanner (Siemens Symphony, Erlangen, Germany) using the standard RF head coil. A slice-selective multiple spin-echo sequence with a CPMG radiofrequency pulse scheme and 32 equidistant spin-echoes was applied (De Deene *et al* 1998b). Other scanning parameters were: echo time $= 20$ ms, repetition time $= 5$ s, resolution $= 192 \times 192$, matrix size $= 192$ mm, slice thickness $= 5$ mm, number of acquisitions $= 2$. R2 maps were obtained by fitting a mono-exponential decay curve to the pixel intensities in the consecutive base images on a pixel-by-pixel basis. For each gel batch, the dose–R2 relationship is established by plotting the average measured R2 in the irradiated part of the test tube as a function of the dose absorbed in that test tube. The sensitivity of the gel α (slope of the dose–R2 curve) was evaluated by applying a linear fit to the dose–R2 data between 1 and 10 Gy.

2.2. Diffusion measurements

A pulsed field-gradient spin-echo (PFGSE) method (Tanner and Stejskal 1968) was used on a benchtop 0.5 T NMR system (Minispec mq20, Bruker, Rheinstetten, Germany) to determine the diffusion coefficient of AA and of the monomer mixture AA and Bis in gels with different gelatin concentrations. For the PFGSE, the attenuation caused by the external applied diffusion gradients is given by

$$\frac{S_g}{S_0} = \exp\left[-\gamma^2\delta^2g^2\left(\Delta - \frac{\delta}{3}\right)D\right] \tag{1}$$

with S_g and S_0 being the measured signal amplitudes respectively with and without a gradient applied, γ being the gyromagnetic ratio, δ being the duration of the gradient pulse, Δ being the time interval between the leading edges of the two gradient pulses, g being the characteristic of the gradient pulse and D being the diffusion coefficient. For this study $\gamma = 42.58$ MHz T^{-1}, $\delta = 1$ ms, $\Delta = 12$ ms and $g \approx 6.8$ T m^{-1}. In order to measure the diffusion coefficient of the monomers in the gel using a PFGSE, signal originating from free water protons should be eliminated. This is achieved by preparing the gel samples with deuterium oxide (99.9% isotopic purity, Sigma-Aldrich, Bornem, Belgium) instead of water.

2.3. Diamond detector measurement

The dose profiles measured in the irradiated test tubes are compared with the dose profile measured with a diamond detector (T60003, PTW, Freiburg, Germany). The dose profile measured with the diamond detector also serves as input for the mathematical model. A relative dose profile in the lateral direction of the 10×10 cm^2 6 MV photon beam was recorded in an automated water phantom system (MP3, PTW, Freiburg, Germany) by using
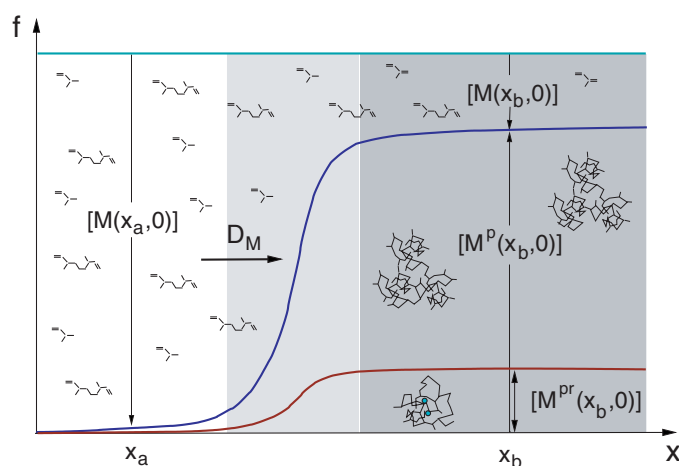
Figure 1. Schematic representation of profiles and the different components present in the gel immediately after irradiation ($t = 0$). Unreacted monomer diffuses into the high-dose region according to its diffusion constant $D_M \cdot [M(x, t)]$, $[M^p(x, t)]$ and $[M^{pr}(x, t)]$ respectively describe the concentrations of monomer, bound monomer and polymer radicals.

the scanning diamond detector. The measurement was performed at a depth of 5 cm at isocentre. To minimize partial volume effects, the diamond detector was oriented for optimal spatial resolution (1 mm). A monitor signal from the accelerator beam monitor was used to correct for measurement errors caused by output rate fluctuations.

2.4. Mathematical model

The underlying hypothesis of the model is that overshoots in the dose profile that occur near high-dose gradients are the result of long-living polymer radicals that recombine with 'fresh' monomers that diffuse from low-dose regions (see figure 1). The differential equation describing this process is given by

$$\frac{\partial [M(x, t)]}{\partial t} = D_M \cdot \frac{\partial^2 [M(x, t)]}{\partial x^2} - k_p \cdot [M(x, t)][M^{pr}(x, t)] \tag{2}$$

with $[M(x, t)]$ and $[M^{pr}(x, t)]$ being the concentration of monomer and polymer radicals at a certain point x and at a certain post-irradiation time t, respectively. D_M is the diffusion coefficient of the monomers in the gel dosimeter and k_p is the reaction rate coefficient of monomers with polymer radical. The polymer radicals are considered to be immobilized by the gel matrix and do not diffuse. The polymer radicals are expressed in terms of the number of monomer units that are contained in the long-living polymer radicals per volume element.

We assume that the concentration of polymer radicals decreases exponentially after irradiation, with a decay constant T_p independent of the monomer concentration according to

$$[M^{pr}(x, t)] = [M^{pr}(x, 0)]_0 \cdot e^{-t/T_p}. \tag{3}$$

No differentiation between the different monomers is considered in this model. However, the proportionality of monomer unit consumption with dose can be regarded as a first-order approximation as derived from first-order chemical kinetics. This assumption is based on the
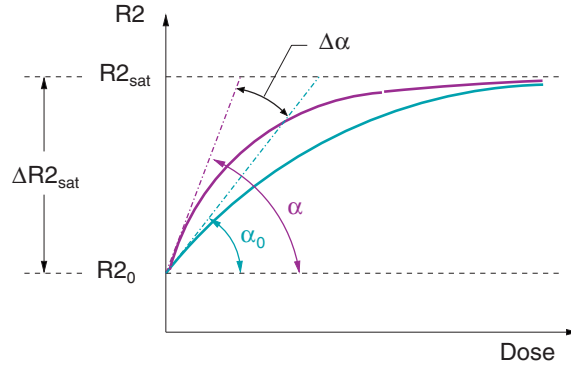
Figure 2. Schematic representation of the change in the dose–R2 curve due to post-irradiation polymerization. In various stability studies, the slope α in the low-dose range of the dose–response curve is plotted as a function of post-irradiation time. The measured R2 in an unirradiated test tube ($R2_0$) and the measured R2 at maximum dose ($R2_{sat}$) are indicated.

exponential decrease in monomer concentration with dose as observed by Fourier transform Raman vibrational spectroscopy (Baldock *et al* 1998). It can be noted that this assumption is only valid within a dose range up to 13 Gy (Jirasek *et al* 2001).

The total concentration of bound monomer units $[M^p(x, t)]$ at a certain time t after irradiation is given by

$$[M^p(x, t)] = [M^p(x, 0)] + \int_0^t k_p \cdot [M(x, t)] \cdot [M^{pr}(x, t)] \cdot dt. \tag{4}$$

When the R2–dose response of the gel dosimeter is determined by using calibration test tubes, the R2 values are extracted from a flat homogeneous dose region. In this region, the monomer concentration is independent of the position x ($\partial[M(x, t)]/\partial x = 0$). As a result, the diffusion term vanishes and equation (2) is reduced to

$$\frac{\partial[M(x_{\text{homog}}, t)]}{\partial t} = -k_p \cdot [M(x_{\text{homog}}, t)][M^{pr}(x_{\text{homog}}, t)] \tag{5}$$

in which x_{homog} stands for all x-positions where the dose distribution is homogeneous. Equation (5) describes the temporal instability in the slope of the dose–R2 response of the polymer gel dosimeter.

Using equation (3), the differential equation (5) is solved for the monomer concentration:

$$[M(x_{\text{homog}}, t)] = [M(x_{\text{homog}}, 0)] \cdot \exp\left(-k_p \cdot [M^{pr}(x_{\text{homog}}, 0)] \cdot T_p \cdot \left(1 - e^{-t/T_p}\right)\right). \tag{6}$$

The change of the dose–R2 curve with post-irradiation time is illustrated in figure 2. The hypothesis on which the model is based also assumes a correlation between the post-irradiation polymerization and the change in slope of the dose–R2 plot. In several stability studies, the change in slope in the quasi-linear region of the dose–R2 curve with post-irradiation time is fitted against a mono-exponential curve (De Deene *et al* 2000, 2002).

$$\alpha = \alpha_0 + \Delta\alpha_\infty \cdot \left(1 - e^{-t/T_p}\right). \tag{7}$$

This fit is applied to extract the dose sensitivity at time $t = 0$ (α_0), the total increase in dose sensitivity ($\Delta\alpha_\infty$) and the macroradical time constant T_p from the measured data. From

figure 2 and equation (6) it can be easily derived that

$$k_p \cdot [M^{\mathrm{pr}}(x, 0)] = \frac{1}{T_p} \cdot \ln\left(\frac{[M(x, 0)]}{[M(x, \infty)]}\right) = \frac{1}{T_p} \cdot \frac{\Delta\alpha_\infty}{(\mathrm{R2_{sat}} - \mathrm{R2_0})} \cdot D(x) \quad (8)$$

with $\mathrm{R2_0}$ being the intercept of the dose–R2 curve at $t = 0$ and $\mathrm{R2_{sat}}$ being the measured R2 at maximum dose. The monomer concentration at all moments after irradiation of a gel dosimeter is obtained by substituting equation (8) into equation (2). The resulting partial differential equation is solved numerically with the finite time increment method (Press *et al* 1992).

The total concentration of bound monomers is obtained by substituting the monomer concentration in equation (4). Substituting equations (3) and (8) into equation (6) yields the monomer concentration in the uniformly irradiated region

$$[M(x_{\mathrm{homog}}, t)] = [M(x_{\mathrm{homog}}, 0)] \cdot \exp\left(-\frac{\Delta\alpha_\infty D(x_{\mathrm{homog}})}{(\mathrm{R2_{sat}} - \mathrm{R2_0})} \cdot \left(1 - \mathrm{e}^{-t/T_p}\right)\right). \quad (9)$$

In this model, we assume that the concentration of bound monomer is proportional to the R2 value.

$$\mathrm{R2} = \mathrm{R2_0} + (\mathrm{R2_{sat}} - \mathrm{R2_0}) \cdot \frac{[M^p(x, t)]}{[M(x, 0)]}. \quad (10)$$

This expression, describing the relation between the monomer concentration and the R2 value, starts from the premise that all monomers are able to react and that the reaction kinetics are independent of the degree of polymerization.

Different coefficients in the model are determined by independent experiments for the different polymer gel compositions. These are:

(i) D_M, the diffusion coefficient of the monomers. The monomer diffusion coefficient depends on the composition of the gel dosimeter and is determined by using independent diffusion measurements (see section 2.2);

(ii) $D(x)$, the one-dimensional dose distribution is measured by using a scanning diamond detector in an automatic water phantom (see section 2.3);

(iii) $\mathrm{R2}(D)$, the dose–R2 relation described by a mono-exponential function with parameters: $\mathrm{R2_0}$, $\mathrm{R2_{sat}}$, α according to $\mathrm{R2}(D) = \mathrm{R2_{sat}} - (\mathrm{R2_{sat}} - \mathrm{R2_0}) \cdot \exp\left(-\frac{\alpha}{\mathrm{R2_{sat}} - \mathrm{R2_0}} \cdot D\right)$ (see section 2.1);

(iv) $\alpha(t)$, the temporal instability of the dose sensitivity due to post-irradiation polymerization with parameters: α_0, $\Delta\alpha_\infty$, T_p according to: $\alpha = \alpha_0 + \Delta\alpha_\infty \cdot (1 - \mathrm{e}^{-t/T_p})$ (see section 2.1).

All simulations are performed on a personal computer with software written in C. All variables have double precision. The time increment and spatial increment for the numerical differentiation and integration were 0.0001 h and 0.5 mm, respectively. Taking smaller time increments or spatial increments did not alter the outcome of the simulations.

3. Results

3.1. Stability study

An R2 image of irradiated test tubes is shown in figure 3(a). The R2 profile in figure 3(b) illustrates an overshoot near the edge of the penumbra. Dose–response curves of the different gel dosimeters, acquired 48 h after irradiation, are given in figure 4. The inset graph shows the correlation between gelatin concentration and dose sensitivity. Increasing the gelatin
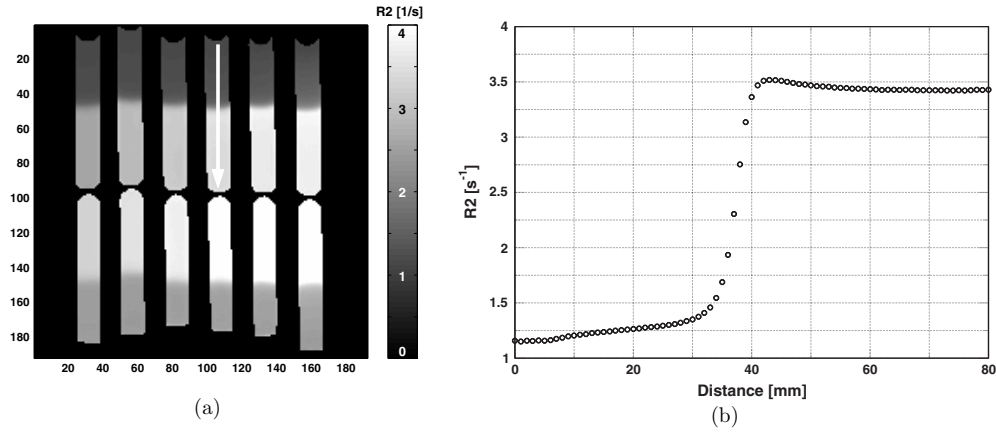
Figure 3. (a) Calculated R2 image of a lengthwise MRI scan of irradiated PAG$_6$ (top) and PAG$_{12}$ (bottom) tubes. The white arrow indicates the orientation of the R2 profile (b). The profile is taken in a PAG$_6$ test tube, 48 h after it was irradiated to a dose of 20 Gy. The edge overshoot is readily observed near the high dose side of the penumbra.
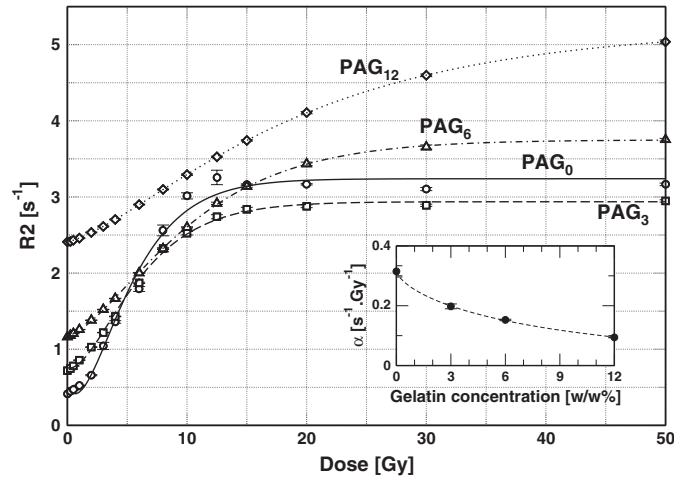

Figure 4. Dose–response curves for the PAG$_0$ (○ ——) , PAG$_3$ (□ – – –), PAG$_6$ (△ — · —) and PAG$_{12}$ (◇ · · ·) gel. Inset graph: correlation between gelatin concentration and dose sensitivity α.

concentration clearly restricts the sensitivity of the dosimeter. Figure 5 displays the dose sensitivity (α) of each polymer gel batch as a function of post-irradiation time. A saturation function (equation (7)) is fitted to the data set of each polymer gel batch to describe the post-irradiation evolution of α. From this fit α_0, $\Delta\alpha_\infty$ and T_p are estimated. All these parameters, together with R2$_0$ and ΔR2$_{sat}$ (= R2$_{sat}$ − R2$_0$) are summarized in table 1. The coefficients α_0 and $\Delta\alpha_\infty$ decrease with increasing gelatin concentration. The parameter ΔR2$_{sat}$ appears to be independent of the gelatin concentration, except for the PAG$_3$ formulation. The change in dose sensitivity $\Delta\alpha_\infty$ for PAG$_6$ is in accordance with previous observations (De Deene *et al* 2000). In figure 6, the time constant T_p is plotted versus the gelatin concentration in the PAG dosimeter. Data points for gelatin concentrations of 5 and 10 (w/w)% are copied from
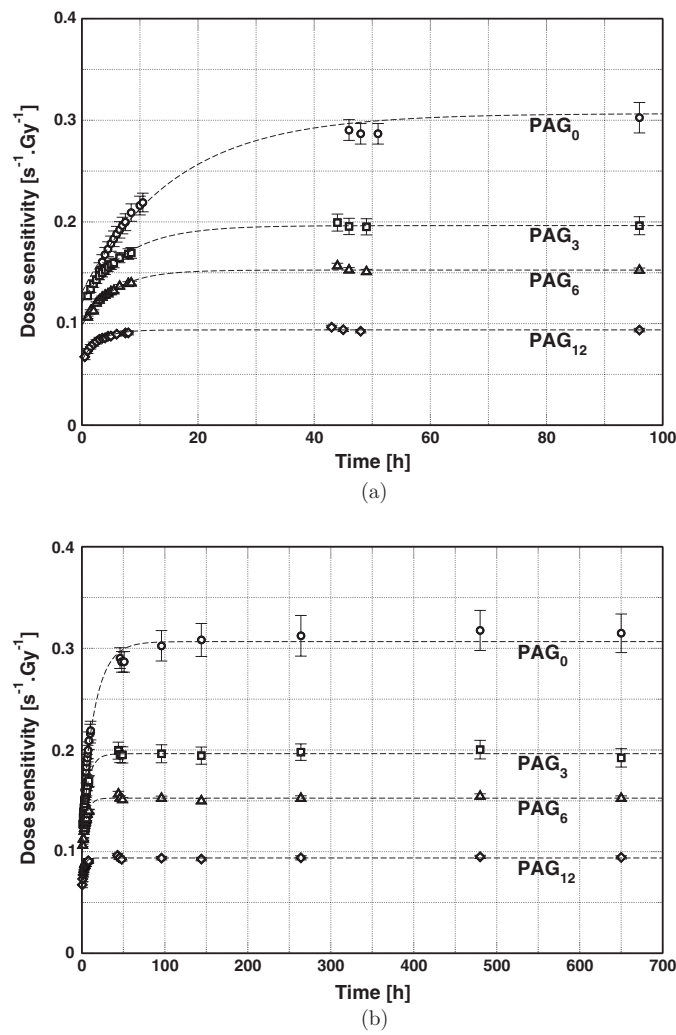
(a)

(b)

Figure 5. Dose sensitivity as a function of post-irradiation time for PAG_0 ($\bigcirc$), PAG_3 ($\square$), PAG_6 ($\triangle$) and PAG_{12} ($\Diamond$). The data are fitted by an exponential saturation function.

Table 1. Measured parameters that describe the dose–R2 relationship of the different gel dosimeters. These parameters are also used as input for the simulations.

	α_0 (s^{-1} Gy^{-1})	$\Delta\alpha_\infty$ (s^{-1} Gy^{-1})	T_p (h)	R2$_0$ (s^{-1})	ΔR2$_{sat}$ (s^{-1})
PAG_0	0.1307	0.1759	15.90	0.42	2.64
PAG_3	0.1207	0.0757	7.54	0.68	2.22
PAG_6	0.0982	0.0544	5.38	1.07	2.62
PAG_{12}	0.0639	0.0299	2.82	2.13	2.65

De Deene *et al* (2002). An exponential decay function is used to fit the decrease of T_p with increasing gelatin concentration. Figure 7 shows R2 profiles (96 h post-irradiation) measured
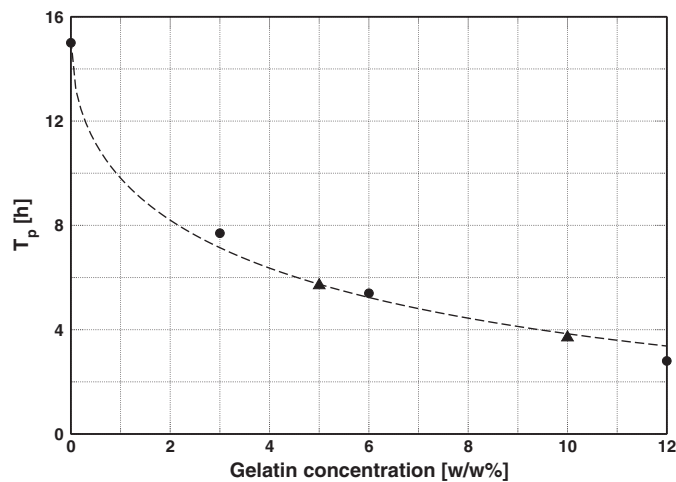
Figure 6. Time constant T_p for the saturation of the dose sensitivity α as a function of gelatin concentration. Data points for 5 and 10 (w/w)% gelatin (▲) are copied from De Deene *et al* (2002).

Table 2. Measured diffusion coefficients of monomers for different gelatin concentrations.

Monomer(s)	3 (w/w)% gelatin	6 (w/w)% gelatin
AA	$(927 \pm 41) \times 10^{-12}$ m^2 s^{-1}	$(610 \pm 46) \times 10^{-12}$ m^2 s^{-1}
AA and Bis	$(543 \pm 13) \times 10^{-12}$ m^2 s^{-1}	$(478 \pm 16) \times 10^{-12}$ m^2 s^{-1}

in test tubes irradiated to different doses (a), and for different gelatin concentrations (b). From these results it is seen that the edge overshoots are more pronounced at higher dose levels, and at lower gelatin concentrations. Other experiments revealed that the overshoot amplitude is independent of the dose rate for dose rates between 50 and 400 cGy min^{-1}.

3.2. Diffusion measurements

The measured diffusion coefficients are given in table 2. A higher gelatin concentration decreases the monomer diffusion coefficient. The diffusion coefficient for the AA and Bis monomer mixture in a 6% gelatin gel agrees with similar measurements performed by Haraldsson *et al* (1999). They also showed that the monomer diffusion coefficient is independent of the amount of polymerization.

3.3. Mathematical simulations

R2 profiles measured at different times after irradiation for a PAG$_3$ and a PAG$_6$ gel (irradiated to 15 Gy and 30 Gy, respectively) are displayed in figure 8(a), (c). These profiles are compensated for the increase in R2 due to the ongoing gelation of gelatin. The overshoots near the beam penumbra can be readily observed after 48 h. No further increase in R2 is noted after this time period. The time-dependent increase in R2 in the high-dose region is related to the post-irradiation polymerization. Figure 8(b), (d) shows a simulation of the cases described above, based on the model parameters from tables 1 and 2. For both cases, good agreement is observed between measurements and simulations.
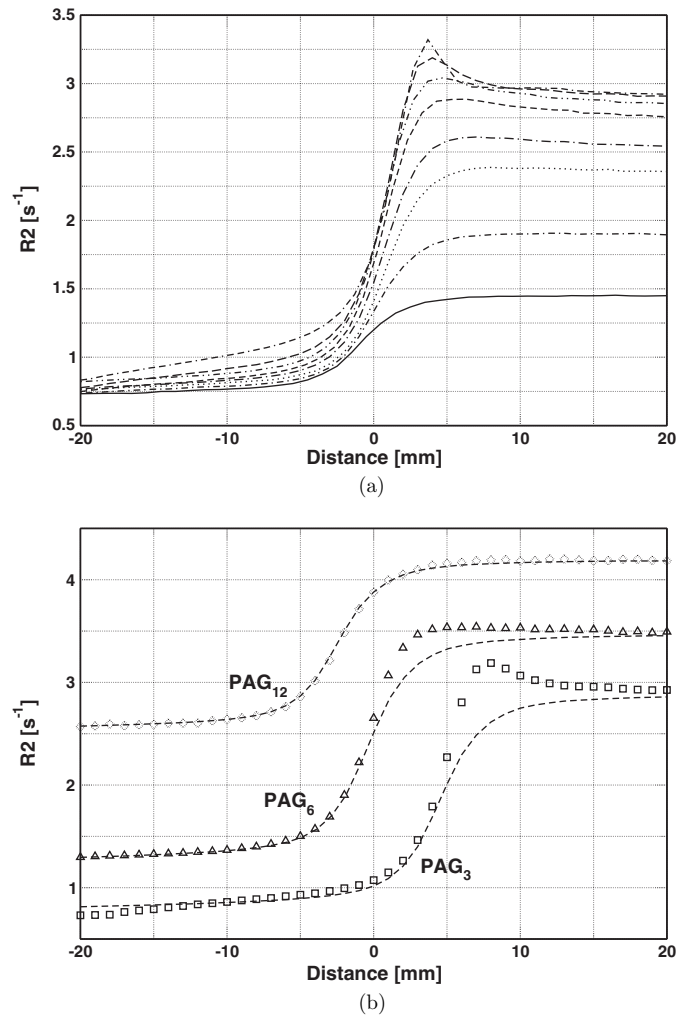
Figure 7. (a) Measured R2 profiles in PAG$_3$ test tubes irradiated to a dose of 4, 6, 8, 10, 12.5, 15, 20 and 30 Gy (from bottom to top). (b) Measured R2 profiles in test tubes irradiated to 20 Gy, for different gelatin concentrations: PAG$_3$ (□), PAG$_6$ (△) and PAG$_{12}$ (◇). The dashed line represents the R2 distribution when diffusion is not taken into account.

Figure 9 shows simulations of irradiated PAG$_6$ gel for different penumbra widths. The penumbra was defined between 10% and 90% of maximum dose. The magnitude of the overshoot decreases with increasing penumbra width. Simulations of the effect of the monomer diffusion coefficient on the overshoot amplitude are shown in figure 10.

In a previous study on temporal and spatial stabilities of polymer gel dosimeters (De Deene *et al* 2002), a PAG-like gel was investigated where AA was replaced by 2-hydroxyethyl acrylate (HEA). A long macroradical lifetime (38 h) was observed in that gel. Also, the measured overshoot relatively decreased with time after it reached its maximum amplitude. Simulations for a case with a high macroradical lifetime are given in figure 11. The simulated overshoot amplitude as a function of post-irradiation time shows qualitative agreement with the observations by De Deene *et al* (2002).
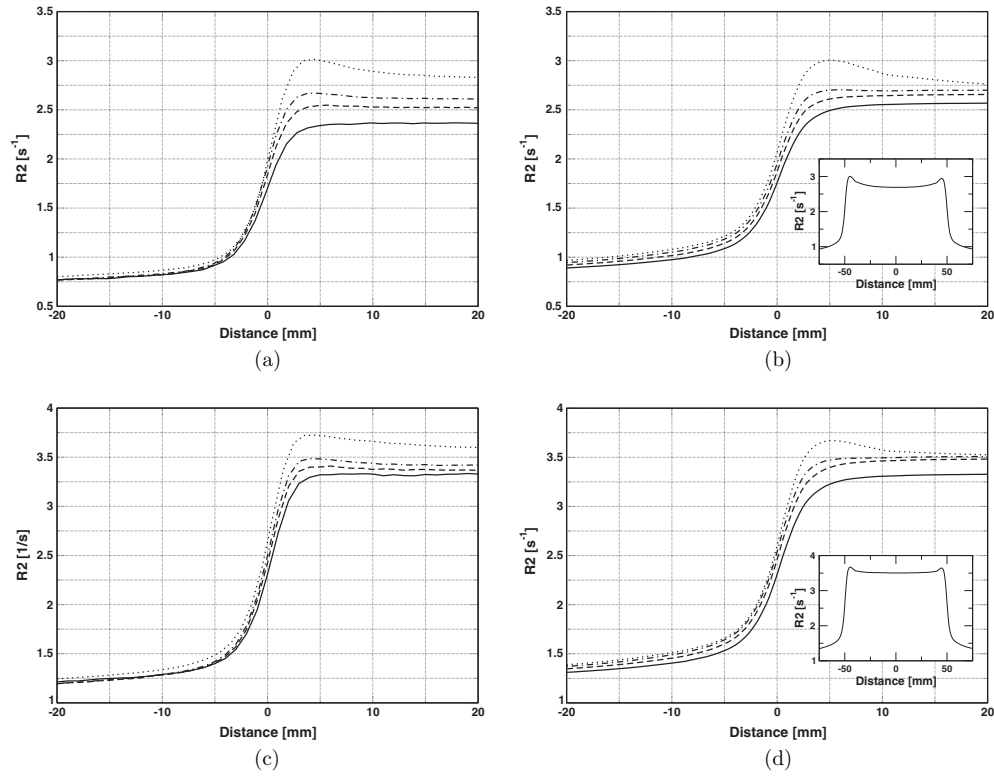
Figure 8. Gel-measured (a), (c) and simulated (b), (d) R2 profiles in the PAG$_3$ (a), (b) and PAG$_6$ (c), (d) gel 1 h (——) , 4 h (– – –), 8 h (— · —) and 48 h (· · ·) after irradiation. The inset graphs show the entire simulated R2 profile 48 h post-irradiation.
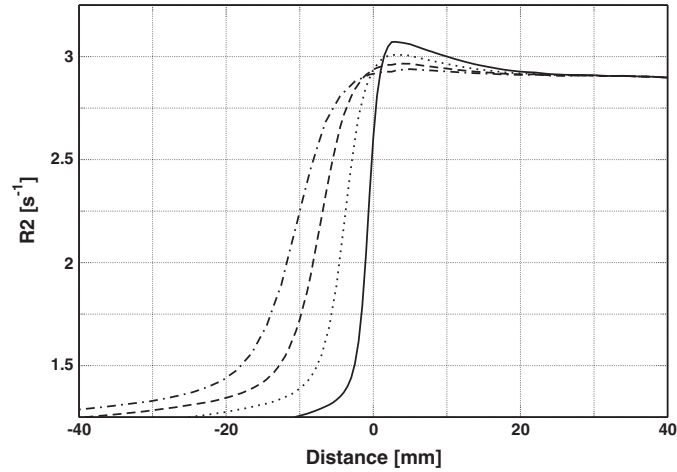

Figure 9. Simulated R2 profiles for the PAG$_6$ gel dosimeter, for a penumbra width of 5.5 mm (——), 11 mm (· · ·), 16.5 mm (– – –) and 22 mm (— · —).

Figure 12 shows measured and simulated dose errors as a consequence of edge overshoots for different doses and different dosimeter gelatin concentrations. The dose errors are
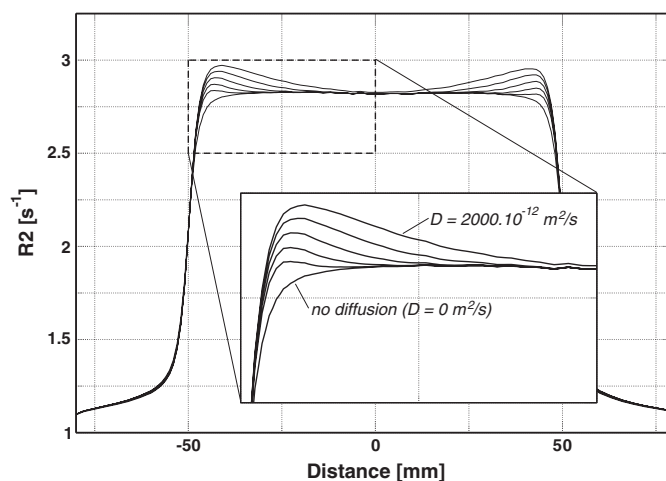
Figure 10. Simulations of R2 profiles for monomer diffusion coefficients of 0, 125, 250, 500, 1000 and 2000 × 10^{-12} m^2 s^{-1}.
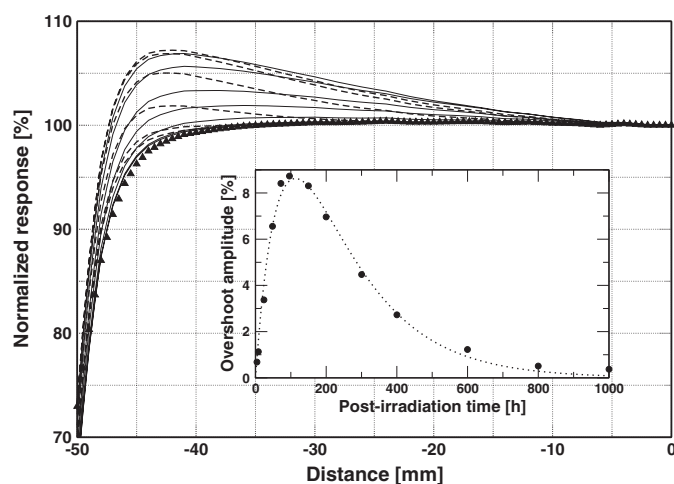

Figure 11. Simulations of R2 profiles in a gel with a long macroradical lifetime (38 h) for different times (4, 8, 24, 48, 72, 96, 150, 200, 300, 400, 600, 800 and 1000 h) post-irradiation. The profiles are normalized to the dose at isocentre, and so the magnitude of the overshoot should be evaluated in a relative fashion. As a reference, the diamond detector measurement is indicated (▲). The overshoot amplitude increases until 96 h after irradiation (dashed lines), and then decreases (full lines). In the inset graph, a bi-exponential fit (dotted line) describes the evolution of the overshoot amplitude as a function of post-irradiation time.

expressed as the maximum relative dose difference between the gel measurement and the diamond detector measurement. No significant overshoots were observed in the PAG_{12} dosimeter, even at high doses. For PAG_3 and PAG_6, dose errors higher than 3% only occur at dose levels above 6 Gy and 8 Gy, respectively. Simulations correlate well with measurements for PAG_6 and PAG_{12}. Based on the experimentally determined input parameters, the model underestimates the dose errors for PAG_3.
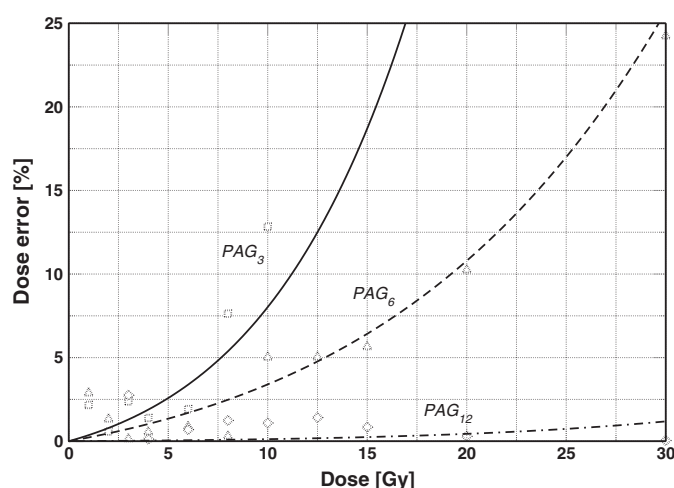
Figure 12. Gel-measured (open symbols) and simulated (lines) maximum relative dose errors in the penumbra region as a consequence of edge overshoots, as a function of absorbed dose for the different gel dosimeters: PAG$_3$ ($\square$——), PAG$_6$ ($\triangle$ – – –) and PAG$_{12}$ ($\Diamond$ — · —).

4. Discussion

The stability study demonstrated an increased dose sensitivity for polymer gel dosimeters with a lower gelatin concentration (figure 4). Computed tomography (CT) analysis of PAG gels also showed an increased sensitivity of gels with lower gelatin concentrations (Trapp *et al* 2001). It is assumed that the propagation and termination rates of radical chain co-polymerization are decreased in the presence of gelatin (Audet 1995). Both propagation and termination reactions are diffusion controlled reactions, and are likely to be affected by the high viscosity of the gelatin solvent. This is confirmed by the diffusion measurements, which showed a decreased monomer diffusion constant for a higher gelatin concentration. Lepage *et al* (2001a) suggested that the initiation rate of the monomers may decrease with increasing gelatin concentration, caused by scavenging of initiating radicals by gelatin. In that paper, it was suggested that the increase in gelatin concentration leads to increased scavenging of initiator fragments and/or increased chain transfer reactions. These ideas have been adapted in a model of the kinetic mechanisms in the PAG dosimeter (Fuxman *et al* 2003). In this model, gelatin is assumed to act as an inhibitor consuming active growing polymer radicals. When the radical time constant T_p is plotted versus gelatin concentration, an exponential decay is observed (figure 6). This confirms that there must be an interaction between gelatin and the polymer macroradicals.

When no gelatin is present in the dosimeter, a quasi-linear dose–R2 relationship is observed up to about 10 Gy (figure 4), depending on the post-irradiation time. A gradual dose-dependent increase in polymer fraction for a gelatin-free PAG dosimeter has also been observed by Park and Schreiner (2001). This is in contradiction with the findings of Maryanski *et al* (1993), who found that the dosimeter reacts as a step-function in the absence of gelatin.

Although polymer gel characteristics such as dose sensitivity and the dose–R2 intercept are clearly influenced by the gelatin content, the maximum increase in R2 (ΔR2$_{\text{sat}}$) appears to be constant for all gelatin concentrations (table 1). The PAG$_3$ dosimeters contained a lower monomer concentration than intended, because part of the monomers did not dissolve and hence were not added to the gelatin solution during gel manufacture. This explains the different ΔR2$_{\text{sat}}$ for PAG$_3$. Because the mathematical model is based on parameters extracted

from gel measurements, the lower monomer concentration in the PAG$_3$ gels is not a source of errors.

Simulations of the time course of the R2 distribution after irradiation agreed with the measurements (figure 8). Quantitative agreement between gel measurements and simulations was also found for the maximum dose error as a function of absorbed dose (figure 12). These results validate our mathematical model, and thereby confirm the hypothesis that the temporal instabilities—as observed in the gel after irradiation—can result in overshoots near the edge of a high-dose gradient. Differences between the simulations and measurements could be due to the fact that the model assumes a mono-exponential dose–R2 relationship, the R2 instability as a consequence of gelatin ageing is not included in the model or incorrect parameters are used in the simulations. The diffusion coefficient of AA alone was used for the simulations. We assumed that Bis does not participate significantly in the creation of overshoots because

(i) Bis is consumed at a higher rate than AA during irradiation so practically no Bis is left at higher doses ($>$15 Gy) (Baldock *et al* 1998, Jirasek *et al* 2001);
(ii) the diffusion coefficient of Bis (200×10^{-12} m^2 s^{-1} for a 6 (w/w)% gel) is significantly lower than that of AA.

For the HEA-gel studied by De Deene *et al* (2002), a long macroradical lifetime was observed. The measured overshoot in that gel reached a maximum after 12 h, after which it started to decrease. Simulations of this case, as shown in figure 11, showed a similar time-dependent behaviour of the overshoot amplitude. The decrease of overshoot amplitude is explained by a continuing influx and polymerization of monomer in the high-dose region. Although the shape of the time course of the overshoots corresponds well with the simulations, the time scale is an order of magnitude longer in the simulations, when compared with the observations made by De Deene *et al* (2002). Assumptions made in the model for PAG dosimeters, such as the relationship between amount of polymer and measured R2, may not be valid for the HEA gel. Still, the qualitative agreement between both curves indicates that a long macroradical lifetime can result in an eventual 'neutralization' of the overshoot.

To assess the applicability of the different gel dosimeters from the point of view of avoiding edge overshoots, the maximum dose error (relative to the given dose) in the measured penumbra was plotted as a function of the delivered dose at isocentre (figure 12). The results demonstrate that a gel dosimeter with high gelatin concentration (and the resulting short macroradical lifetime) is less susceptible to spatial instabilities. However, other dosimeter characteristics (such as temperature and dose rate dependence) might be affected by the high gelatin content. Investigation of these factors was beyond the scope of this study.

This work demonstrated that the magnitude and shape of the overshoots are determined by the diffusion constant of the monomer and the macroradical lifetime (both determined by the gelatin concentration), the absorbed dose, the dose–R2 relationship and its instability, the penumbra width and the time after irradiation.

5. Conclusions

A mathematical model to predict the time-dependent post-irradiation evolution of the measured R2 and dose distribution in PAG polymer gel dosimeters is proposed. The model is based on the hypothesis that macroradicals are responsible for both temporal and spatial instabilities observed in the polymer gel after irradiation. Comparison of experimental data with simulations validates the relation between the temporal instability and the spatial dose integrity, supporting our hypothesis. This model can be applied to quantitatively predict the overshoot amplitude in a gel-measured dose distribution.

Results also suggest an effect of gelatin on the post-irradiation polymerization process. Increasing the gelatin concentration in a polymer gel dosimeter decreases the monomer diffusion constant and the macroradical lifetime. As a result, a decrease in both the dose sensitivity and overshoot susceptibility is observed in a polymer gel with increased gelatin content.

This study shows that with respect to the spatial and temporal stabilities of polymer gel dosimeters, it is advisable to use monomers with a low diffusion coefficient and with short macroradical lifetime. Alternatively other gelling agents that decrease the monomer diffusion can be used. The theoretical model provided in this study can be used as a predictive tool to optimize the gel dosimeter composition with respect to the temporal and spatial stabilities.

Acknowledgments

References

Audet C 1995 NMR-dose response studies of the gels used for 3D radiation dosimetry by magnetic resonance imaging *PhD Thesis* McGill University, Montréal

Baldock C, Lepage M, Rintoul L, Murry P and Whittaker A K 1999 Investigation of polymerisation of radiation dosimetry polymer gels *Proc. 1st Int. Workshop on Radiation Therapy Gel Dosimetry (Lexington, Kentucky)* ed L J Schreiner pp 99–105

Baldock C, Rintoul L, Keevil S F, Pope J M and George G A 1998 Fourier transform Raman spectroscopy of polyacrylamide gels (PAGs) for radiation dosimetry *Phys. Med. Biol.* **43** 3617–27

De Deene Y, De Wagter C, Van Duyse B, Derycke S, De Neve W and Achten E 1998a Three-dimensional dosimetry using polymer gel and magnetic resonance imaging applied to the verification of conformal radiation therapy in head-and-neck cancer *Radiother. Oncol.* **48** 283–91

De Deene Y, Hanselaer P, De Wagter C, Achten E and De Neve W 2000 An investigation of the chemical stability of a monomer/polymer gel dosimeter *Phys. Med. Biol.* **45** 859–78

De Deene Y, Reynaert N and De Wagter C 2001 On the accuracy of monomer/polymer gel dosimetry in the proximity of a high-dose-rate ^{192}Ir source *Phys. Med. Biol.* **46** 2801–25

De Deene Y, Van de Walle R, Achten E and De Wagter C 1998b Mathematical analysis and experimental investigation of noise in quantitative magnetic resonance imaging applied to polymer gel dosimetry *Signal Process* **70** 85–101

De Deene Y, Venning A, Hurley C, Healy B J and Baldock C 2002 Dose-response stability and integrity of the dose distribution of various polymer gel dosimeters *Phys. Med. Biol.* **47** 2459–70

Fuxman A M, McAuley K B and Schreiner L J 2003 Modeling of free-radical crosslinking copolymerization of acrylamide and N, N′-methylenebis(acrylamide) for radiation dosimetry *Macromol. Theory Simul.* **12** 647–62

Haraldsson P, Nydén M, Bäck S Å J and Olsson L E 1999 Characterization of radiation induced polymer in dosimeter gel *Proc. 1st Int. Workshop on Radiation Therapy Gel Dosimetry (Lexington, Kentucky)* ed L J Schreiner pp 121–3

Hoecker F E and Watkins I W 1958 Radiation polymerization dosimetry *Int. J. Appl. Radiat. Isot.* **3** 31–3

Jirasek A I, Duzenli C, Audet C and Eldridge J 2001 Characterization of monomer/crosslinker consumption and polymer formation observed in FT-Raman spectra of irradiated polyacrylamide gels *Phys. Med. Biol.* **46** 151–65

Lepage M, Whittaker A K, Rintoul L, Bäck S Å J and Baldock C 2001a The relationship between radiation-induced chemical processes and transverse relaxation times in polymer gel dosimeters *Phys. Med. Biol.* **46** 1061–74

Lepage M, Whittaker A K, Rintoul L, Bäck S Å J and Baldock C 2001b Modelling of post-irradiation events in polymer gel dosimeters *Phys. Med. Biol.* **46** 2827–39

Maryanski M J, Gore J C, Kennan R P and Schulz R J 1993 NMR relaxation enhancement in gels polymerized and cross-linked by ionizing radiation: a new approach to 3D dosimetry by MRI *Magn. Reson. Imaging* **11** 253–8

Maryanski M J, Schulz R J, Ibbott G S, Gatenby J C, Xie J, Horton D and Gore J C 1994 Magnetic resonance imaging of radiation dose distributions using a polymer-gel dosimeter *Phys. Med. Biol.* **39** 1437–55

Park Y S and Schreiner L J 2001 Basic investigations of an aqueous polyacrylamide dosimeter without gelatin *Proc. 2nd Int. Conf. on Radiotherapy Gel Dosimetry (Brisbane)* ed C Baldock and Y De Deene pp 107–9

Press W H, Teukolsky S A, Vetterling W T and Flannery B P 1992 *Numerical Recipes in C—The Art of Scientific Computing* 2nd edn (Cambridge: Cambridge University Press) p 827

Tanner J E and Stejskal E O 1968 Restricted self-diffusion of protons in colloidal systems by the pulsed-gradient, spin-echo method *J. Chem. Phys.* **49** 1768–77

Trapp J, Bäck S Å J, Lepage M, Michael G and Baldock C 2001 An experimental study of the dose response of polymer gel dosimeters imaged with x-ray computed tomography *Phys. Med. Biol.* **46** 2939–51

Vergote K, De Deene Y, Duthoy W, De Gersem W, De Neve W, Achten E and De Wagter C 2004 Validation and application of polymer gel dosimetry for the dose verification of an intensity-modulated arc therapy (IMAT) treatment *Phys. Med. Biol.* **49** 287–305